Jestr

Journal of Engineering Science and Technology Review 17 (4) (2024) 9 – 15

Research Article

JOURNAL OF
Engineering Science and Technology Review

www.jestr.org

Water Temperature Changes on Performance of Magnesium Oxysulfate-based Yellow Gypsum Foam Concrete

Shuren Wang[1,2], Yan Wang[1], Jian Gong[1,*] and Linru Zhao[1]

[1]*School of Civil Engineering, Henan Polytechnic University, Jiaozuo 454003, China*
[2]*Collaborative Innovation Center of Coal Work Safety and Clean High-Efficiency Utilization, Henan Polytechnic University, Jiaozuo 454003, China*

Received 15 May 2024; Accepted 23 August 2024

Abstract

To promote the reuse of yellow gypsum (YG), an industrial solid waste, and achieve energy savings and environmental protection, the impact of water temperature variation on the performance of magnesium oxysulfate-based yellow gypsum (YG-MOS) foamed concrete was investigated. YG-MOS foamed concrete was prepared using magnesium oxysulfate (MOS) foamed cement as the matrix and YG as the admixture, with water at varying temperatures. This study aimed to elucidate how changes in water temperature affect the properties of YG-MOS foamed concrete. Results show that, after a 28-day curing period, as the water temperature increases, the compressive strength, dry density, and thermal conductivity of the samples initially rise but subsequently decline. These properties reach their peak values when the water temperature is 35 °C. Additionally, as the water temperature rises, the porosity of the samples first decreases and then increases, with the minimum porosity observed at 35 °C. At this temperature, the mean pore size and its standard deviation are also minimized, resulting in the most uniform pore size distribution. Furthermore, as the temperature varies between 35 °C and 60 °C, the concentration of the 5-phase $5Mg(OH)_2 \cdot MgSO_4 \cdot 7H_2O$ in the sample gradually decreases, while the formation of flake, cluster, and petal-like magnesium hydroxide structures significantly increases. These findings provide valuable insights for the application of YG-MOS foamed concrete in civil engineering.

Keywords: Foamed concrete, Magnesium oxysulfate, Yellow gypsum, Microscopic analysis, Water temperature

1. Introduction

Yellow gypsum (YG), also known as titanium gypsum, is a yellow block of industrial solid waste produced during the production of titanium dioxide via the sulfuric acid method. Its main component is $CaSO_4 \cdot 2H_2O$. Each ton of titanium dioxide produced through the sulfuric acid method generates 6-10 t of YG waste residue. Currently, the annual production of YG in China is nearly 30 Mt, but the utilization rate is less than 10% [1, 2]. The industrial sector is developing rapidly, and the output of YG is also increasing annually. YG has complex components and contains a variety of metal elements, which also makes the treatment of YG more difficult. At present, there are two main ways to address YG. First, although YG is reused through a process, the process is complex, and the reuse rate of YG is low. Second, YG is buried or stacked as industrial waste, which is also the main treatment method for YG at present.

Foam concrete in China is mostly made of Portland cement mixed with sand and other materials to prepare slurries, and foam is introduced into it. Due to the shortcomings of low early strength in foam concrete, its application has been limited to varying degrees. Therefore, lightweight foam thermal insulation materials have received extensive attention as a new type of environmentally friendly thermal insulation building material. Lightweight foam thermal insulation materials are a new type of lightweight porous thermal insulation cementitious material prepared by adding other lightweight aggregates, modifiers, and other admixtures to cement as the main cementitious material through physical foaming of foam or chemical foaming of chemical foaming agents. They have the advantages of low dry density, low thermal conductivity, excellent sound insulation performance, and good fire resistance [3].

As a magnesium-based gas-hardened cementitious material, magnesium oxysulfate cement (MOS) has the advantages of low dry density, low thermal conductivity, low alkalinity, high early strength, and good fire resistance. It has gradually become widely used in the preparation of lightweight foam thermal insulation materials [4]. Foam MOS is a porous gas-hardened cementitious material made by physical or chemical foaming, stirring, injection molding, standing, mold removal, and curing. However, there are also several problems in practical preparation and application, such as inadequate water resistance, susceptibility to collapse and cracking, and low strength.

2. State of the Art

The treatment of industrial solid waste will be a significant issue in the future. To promote the concepts of sustainable development, energy conservation, and environmental protection, and to safeguard our homes and the environment, we must address industrial solid waste in an efficient, green, and energy-saving manner [5-7]. Currently, YG is often landfilled as industrial waste [8, 9]. However, YG contains various compounds and is weakly acidic. As a landfill material, it can severely pollute the environment and have detrimental effects on the local ecological system [10, 11].

*E-mail address: gongjian@hpu.edu.cn
ISSN: 1791-2377
doi:10.25103/jestr.174.02

Numerous scholars have researched how to utilize YG effectively and sensibly. Some studies have reported that incorporating an appropriate amount of YG into MOS can significantly reduce the setting time and increase strength. For instance, Rosli et al. [12] developed a novel material by blending sludge and red gypsum, which can serve as a landfill cover and exhibits good compressive strength and plasticity. Sotiriadis et al. [13] produced YG as a gypsum-cement-pozzolanic binder with self-cleaning capabilities. Many scholars have applied YG in construction, finding that combining yellow gypsum with cement concrete enhances the incorporation of YG. Wang et al. [14] noted that adding YG to magnesium oxychloride cement (MOC) boosts its compressive strength and ductility. Gu et al. [15] used untreated desulfurized gypsum to replace MgSO4 in magnesium oxysulfate cement (MOS) to prepare MOS. This incorporation of gypsum effectively improved the compressive strength, water resistance, and volume stability of the material.

Compared with traditional Portland cement, MOS is considered a new type of environmentally friendly material due to its lower carbon dioxide emissions, which has attracted increasing attention. Domestic and foreign scholars have conducted numerous studies on MOS. Li et al. [16] reported that flue gas desulfurized gypsum was incorporated into MOS, and the compressive strength of MOS cured at 40 °C for 28 d reached 56.6 MPa, which was a 12.5% increase compared with that of MOS cured at 20 °C. Fang et al. [17] investigated the impact of curing at low temperatures on the properties of basic magnesium sulfate cement. They reported that lower temperatures decreased the crystallinity of the 5-phase $5Mg(OH)_2 \cdot MgSO_4 \cdot 7H_2O$, thereby increasing its water solubility. As a consequence, basic magnesium sulfate cement exhibited reduced water resistance. The temperature significantly affects the performance of MOS. Rodríguez-Alfaro et al. [18] found that 3-phase ($3Mg(OH)_2 \cdot MgCl_2 \cdot 8H_2O$), with a needle-like morphology, was the primary crystallized hydration product for MOC composites. Dionisio and Gomes [19] reported that the state of the 3-phases is not stable under ambient temperature conditions. Li et al. [20] found that adding red mud and iron tailings into MOS to prepare foamed concrete has good economic benefits. Jiang et al. [21] reported that the incorporation of rice straw into MOS-based foamed lightweight insulation materials effectively improved the dry shrinkage, thermal conductivity, and flexural strength of these materials. Temperature affects important factors such as the porosity of foamed concrete, but there are few studies on the influence of water temperature on MOS foamed concrete, which requires further investigation.

In this work, YG industrial solid waste was mixed into MOS as an admixture, and YG-MOS foamed concrete was prepared using water at different temperatures. The effect of water temperature on the performance of YG-MOS foamed concrete was investigated. MOC foam cement was used as the basic raw material, and YG was used as the admixture. The effects of different water temperatures on the properties of YG-MOS foamed concrete were studied. The effects of different water temperatures on the compressive strength, thermal conductivity, dry density, porosity, pore size, phase composition, and microstructure of YG-MOS foamed concrete were analyzed using a universal testing machine, X-ray diffraction (XRD), Scanning Electron Microscope (SEM), and ImageJ software [22].

The remainder of this study is organized as follows: Section 3 outlines the experimental materials, procedures, and test methods for YG-MOS foamed concrete. Section 4 presents an analysis and discussion of the experimental findings. Finally, Section 5 summarizes the experimental results and analysis.

3. Methodology

3.1 Test Materials

In this study, the light-burned magnesium oxide (MgO) had a purity of 85%. It was produced in Dashiqiao, located in Yingkou city, China. According to X-ray fluorescence (XRF) analysis, the content of MgO was ≥ 85%, with a small amount of impurities including MnO, SiO_2, CaO, and other substances. The standard hydration reaction of MgO used to measure the content of active MgO yielded a result of 63.5%, as detailed in Table 1. The $MgSO_4 \cdot 7H_2O$ used in the study was produced by Shanghai Minhang Shenlong Light Chemical Co., Ltd., with an effective content of ≥ 99%. The primary chemical components and their respective contents are presented in Table 2.

YG, a brown-yellow block, was sourced from Baililian Light Chemical Co., Ltd., located in Jiaozuo city, China. To determine the main chemical composition and content of YG, XRF and XRD techniques were employed. The results are shown in Table 3 and Fig. 1, respectively.

The foaming agent used was hydrogen peroxide (H_2O_2) with a concentration of 30%, sourced from our laboratory. Additionally, citric acid and MnO, both of analytical purity, were produced by National Pharmaceutical Group Chemical Reagents Co., Ltd..

Table 1. Chemical composition of MgO

Ingredient	MgO	MnO	SiO_2	CaO	Al_2O_3	Fe_2O_3	SO_3	Active
Content (%)	85.95	6.73	3.62	2.23	0.62	0.48	0.22	63.5%

Table 2. Chemical composition of $MgSO_4 \cdot 7H_2O$

Ingredient	$MgSO_4 \cdot 7H_2O$	$MgSO_4$	MgO	Mg	Cl	Fe
Content (%)	99.50	48.59	16.20	9.80	0.03	0.005

Table 3. Chemical composition of YG

Ingredient	SO_3	CaO	Fe_2O_3	SiO_2	Al_2O_3	MgO	Na_2O	MnO	Other
Content (%)	38.50	30.16	13.62	3.62	3.30	1.74	0.95	0.65	4.96

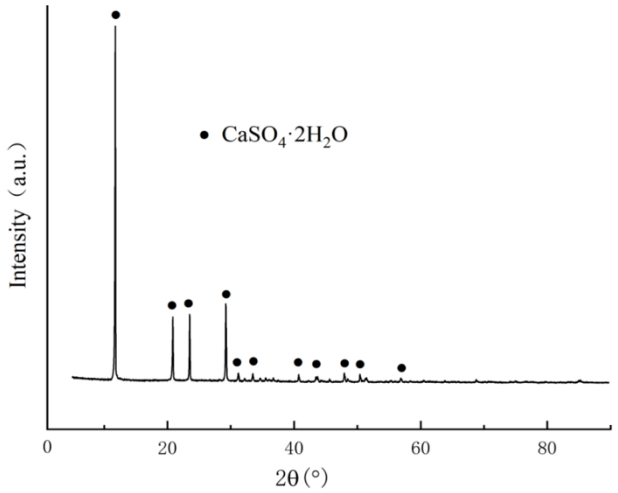

Fig. 1. XRD analysis of YG

3.2 Experimentation

To investigate the impact of experimental water temperature on MOS, the molar ratio of MOS in this experiment was fixed at 8:1:20, and the amount of YG was 6% of the mass of MgO. MOS was prepared using water at various temperatures: 5 °C, 10 °C, 15 °C, 20 °C, 25 °C, 30 °C, 35 °C, 40 °C, 45 °C, 50 °C, 55 °C, and 60 °C. First, the block of YG was dehydrated and manually broken into small pieces. The samples were then crushed into a powder using a crusher, sieved through a 200-mesh square sieve, and sealed for preservation. Before starting the experiment, a bucket was filled with tap water, which was then heated to a specific temperature.

Initially, YG, MgO, and MnO_2 were weighed and added to a mixer. The mixture was stirred for 300 s to ensure thorough blending. Subsequently, citric acid and $MgSO_4 \cdot 7H_2O$ were added to the barrel, followed by water heated to the desired temperature. The mixture was stirred thoroughly again. The resulting solution was then poured over the dry material and stirred for 120 s until fully mixed. H_2O_2 was added, and the mixture was stirred for an additional 30 s before being poured into a cube-shaped mold with an edge length of 100 mm. After 24 h, the test block was removed from the mold and placed in a room maintained at a temperature of 23 ± 3 °C and a relative humidity of 50 ± 5% for curing.

3.3 Test methods

The test methods for determining sample properties are as follows:

Compressive Strength Test: An electronic universal testing machine with a loading rate of 0.5 kN/s was used to measure the compressive strength of cube specimens with an edge length of 100 mm, which had been cured for different durations.

Thermal Conductivity Test: A cube sample that had been cured for 28 d was cut into a sheet-like square with a side length of 100 mm and a thickness of 10 mm. A thermal conductivity tester was then used to measure the thermal conductivity of this sample.

Surface Porosity Test: The surface profile of the sample was photographed, and the resulting image was analyzed using ImageJ software to determine the surface porosity.

Dry Density Test: The dry density of the samples was tested according to the Chinese standard JG/T 266-2011 for foam concrete.

Hole structure test: The sample profile was photographed, and the image was analyzed via ImageJ software.

4. Results analysis and discussion

4.1 Effect of water temperature change on strength of YG-MOS foam concrete

Fig. 2 illustrates the impact of varying water temperatures on the compressive strength of YG-MOS foamed concrete. As the water temperature increases, the strength initially rises to a peak value before subsequently declining. When the curing time is 24 h and 3 d, the strength curve is undulating, and there is no discernible trend in strength change. With a curing time of 7 d, the strength curve rises initially but then decreases. At 35 °C, the sample attains its peak compressive strength of 4.16 MPa, representing a 39.3% increase compared to that at 5 °C. For a curing time of 14 d, the peak strength occurs at 30 °C, achieving a compressive strength of 4.31 MPa, which is 23.1% higher than that at 5 °C. When the curing time is extended to 28 d, the maximum strength of 4.67 MPa is observed at 35 °C, a 29% increase over the strength at 5 °C. Analysis of the experimental data reveals that while water temperature has a minimal effect on early strength, it significantly influences later strength in YG-MOS foam concrete.

As the experimental water temperature rises, the strength gradually decreases; this is because the temperature within the test block becomes too high, causing the reaction rate in the system to accelerate excessively. The heat generated in the test piece dissipates too slowly, resulting in a loose and unstable structure within the test piece, leading to extremely low strength. When the water temperature is between 5-15 °C, the temperature within the sample is low and fails to provide a sustained temperature for the reaction within the system, leading to a low reaction rate and subsequently low sample strength. Conversely, in the experimental temperature range of 30 °C to 40 °C, the samples exhibit a moderate reaction rate, uniform pore distribution, and high strength.

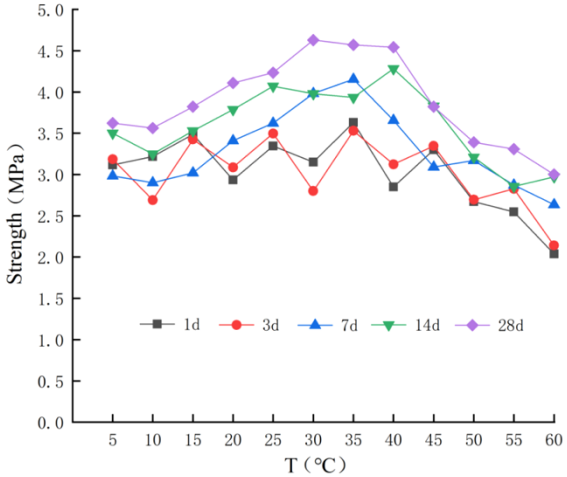

Fig. 2. Compressive strength curves of YG-MOS foam concrete at different water temperatures

4.2 Effects of water temperature changes on the porosity and dry density of YG-MOS foam concrete

To understand the influence of water temperature on the porosity and dry density of YG-MOS foamed concrete, after 28 d of curing, the 100 mm cube samples were placed in a

drying oven and dried until they reached a constant weight. Subsequently, the dry density of the samples was calculated based on their weight. The samples were then sliced, and the sections were photographed. The images were measured and analyzed using ImageJ software to obtain the surface porosities of the samples. The relationship between the dry density and porosity of the samples is depicted in Fig. 3.

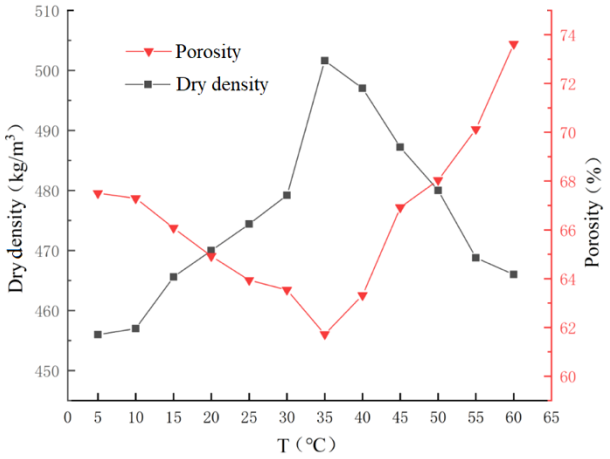

Fig. 3. Relationship curves between dry density and porosity of YG-MOS foam concrete at different water temperatures

Fig. 3 illustrates that the dry density curve and porosity curve of the samples exhibit opposite growth trends. This phenomenon can be attributed to the varying solubilities of $MgSO_4·7H_2O$ in water at different temperatures. When the temperature is below 35 °C, $MgSO_4·7H_2O$ does not fully dissolve in water. As the temperature increases, the solubility of $MgSO_4·7H_2O$ gradually improves. This increased solubility results in more $MgSO_4·7H_2O$ participating in chemical reactions within the foam concrete mixture. Consequently, several effects occur: the viscosity of the foam concrete increases, the size of the pores within the foam concrete decreases, and as a result, the dry density of the sample gradually increases. This trend continues until a certain point, after which further temperature increases may cause excessive $MgSO_4·7H_2O$ to dissolve, potentially reducing its participation in reactions and thus leading to a decrease in dry density. In summary, the complex interplay between $MgSO_4·7H_2O$ solubility, chemical reactions, foam viscosity, and pore structure changes with temperature accounts for the observed variation in the dry density of the samples.

At 5 °C, the dry density of the sample is 456 kg/m³, whereas at 35 °C, the dry density peaks at 501.6 kg/m³, representing a 10% increase from the density observed at 5 °C. According to Chinese standard JG/T 266-2011 Foam Concrete, the sample conforms to the A05 dry density grade. As for porosity, at 5 °C, it is 67.3%, which decreases as the temperature increases. Specifically, at 35 °C, the porosity reaches its minimum value of 61.72%, marking an 8.3% decrease from that at 5 °C. However, as the temperature further increases to 60 °C, the porosity increases to 73.62%, which is 19.3% higher than at 35 °C. This variation can be attributed to the changing solubility of $MgSO_4·7H_2O$ with temperature. As the temperature rises, the solubility of $MgSO_4·7H_2O$ increases, enhancing the solution concentration and potentially reducing the effectiveness of the foaming agent. This results in smaller pore sizes at intermediate temperatures like 35 °C, where $MgSO_4·7H_2O$ fully dissolves and maximizes the solution concentration. However, beyond this optimal temperature, the further increase in temperature may stimulate additional foaming activity, leading to the formation of larger pores and an increase in porosity.

4.3 Effect of water temperature change on thermal conductivity of YG-MOS foam concrete

The thermal conductivity of the sample, cured for 28 d, is measured as shown in Fig. 4. The thermal conductivity of the sample tends to increase until the water temperature reaches 35 °C. After that, the thermal conductivity of the sample initially increases notably but then decreases as the water temperature further increases.

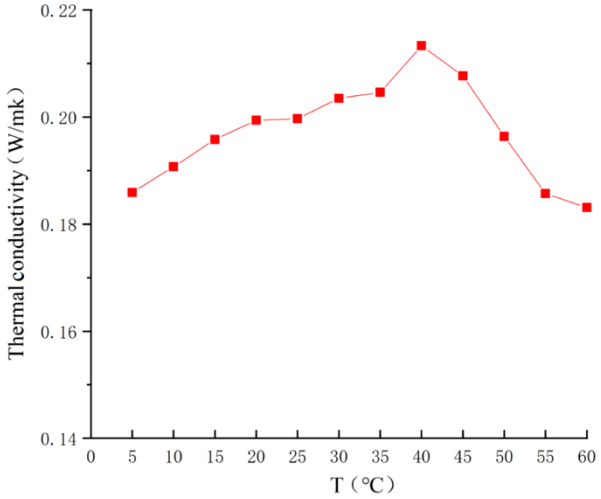

Fig. 4. Thermal conductivity curve of YG-MOS foam concrete at different water temperatures

The experimental results show that as the water temperature increases, the solubility of $MgSO_4·7H_2O$ enhances, leading to an increase in the viscosity of the cement paste and a decrease in the foaming rate. Consequently, the pore size and porosity of the bubbles within the specimen decrease, contributing to an increase in the thermal conductivity of the specimen. At 35 °C, $MgSO_4·7H_2O$ is fully dissolved in the water. Beyond this point, as the water temperature continues to rise, the foaming rate increases, resulting in larger bubble pore sizes and higher porosity in the sample. These changes gradually decrease the thermal conductivity of the sample, which aligns with the previous analysis regarding the effects of time, porosity, and pore size.

4.4 Effect of water temperature change on the pore size of YG-MOS foam concrete

After the sample was cured for 28 d, it was sliced, and the section was photographed. A uniform area of the cellular structure was selected, and a 30 mm × 30 mm image was intercepted. ImageJ software was utilized to measure and analyze the intercepted images. Fig. 5 depicts the relationship between the average pore diameter and the standard deviation of YG-MOS foam concrete at varying water temperatures, while Fig. 6 illustrates the pore size distribution.

Figs. 5 and 6 reveal that both the average pore diameter and the standard deviation initially decrease and then increase with the rise in water temperature. At 5 °C, the average pore diameter measures 2.22 mm. As the experimental water temperature escalates, this diameter decreases, attaining a minimum of 1.84 mm at 35 °C, which is 16.8% lower than the value at 5 °C. Correspondingly, the standard deviation of the pore diameter reaches its nadir,

signifying more uniform pore sizes and a denser, more homogeneous structure within the sample. This observation is congruent with the analysis of compressive strength and dry density.

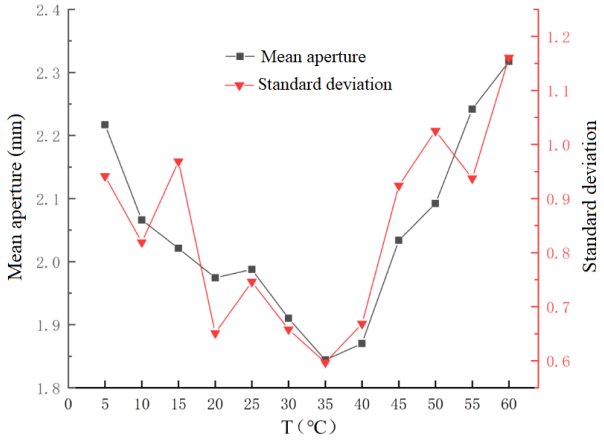

Fig. 5. Relationship curves between mean aperture and standard deviation of pore size of YG-MOS foam concrete

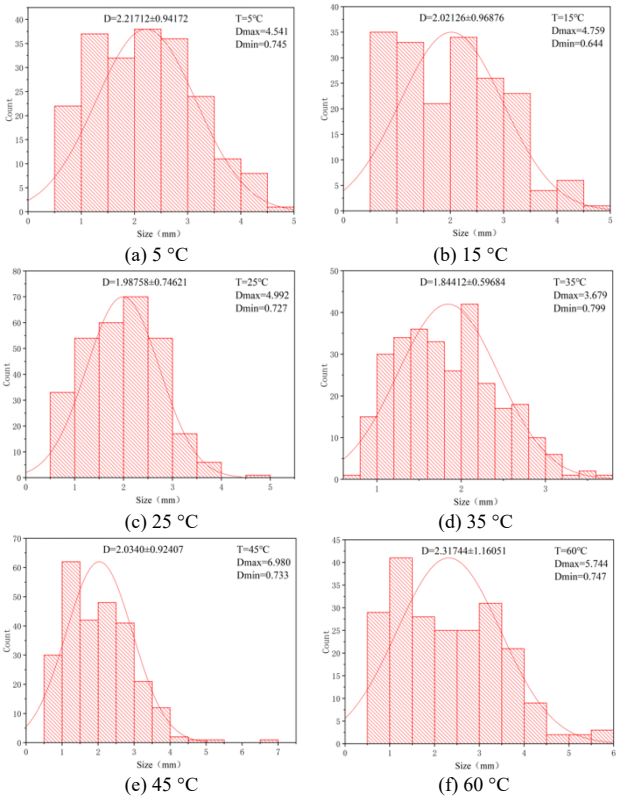

Fig. 6. Distribution of pore size of YG-MOS foam concrete at different water temperatures

However, beyond 35 °C, as the temperature continues to soar up to 60 °C, the trend reverses. This phenomenon can be attributed to the complete dissolution of $MgSO_4·7H_2O$ in water at 35 °C. With further temperature increases, the reaction rate of the foaming agent accelerates, enhancing the rate of bubble formation and leading to the emergence of numerous large-aperture bubbles. The presence of these large bubbles disrupts the uniformity of pore distribution within the sample, causing an increase in porosity and dry density, while simultaneously decreasing the compressive strength at 60 °C. Both the average pore diameter and its standard deviation peak at their maximum values at this temperature, with the mean pore diameter reaching 2.32 mm, a 25.7% surge from the value at 35 °C. This enlargement of pore diameter, coupled with a decrease in sample density and uneven local bubble distribution, contributes to the decline in compressive strength and dry density, and an elevation in porosity, all of which align with the analysis of the previously mentioned experimental outcomes.

4.5 XRD analysis of YG-MOS foam concrete under different water temperatures

The XRD analysis results of YG-MOS foamed concrete, after 28 d of curing in air at various experimental water temperatures, are presented in Fig. 7.

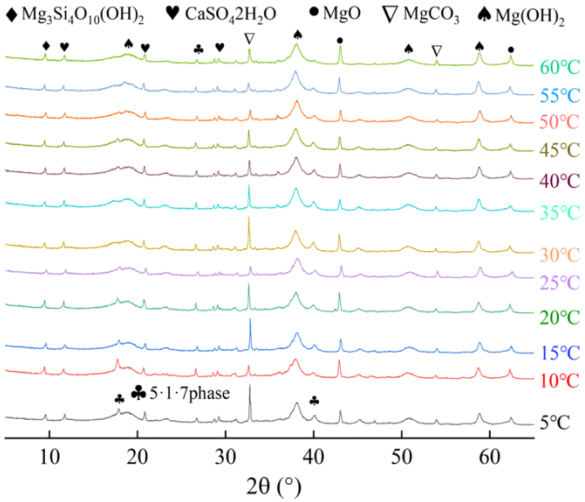

Fig. 7. XRD patterns of YG-MOS foam concrete at different water temperatures

According to the XRD analysis, the hydration products of YG-MOS foamed concrete are primarily constituted by a small amount of a 5-phase mixture comprising $Mg(OH)_2$, $MgCO_3$, MgO, $CaSO_4·2H_2O$, and a trace of magnesium silicate hydrate. This 5-phase blend serves as the primary hydration product in the ternary system, characterized by its stable structure. Conversely, the 3-phase material is metastable under ambient temperature curing conditions and fails to maintain stability. Consequently, MOS exhibits a porous, loose morphology dominated by $Mg(OH)_2$. MgO originates from the experimental raw material, while $CaSO_4·2H_2O$ stems from YG. $MgCO_3$ is generated through the interaction of $Mg(OH)_2$ with CO_2 present in the air. Additionally, hydrous magnesium silicate arises from the reaction between SiO_2 in YG and a minute quantity of dolomite present in the raw material. The reaction equation governing this process is provided in Eq. (1). interests of leading members.

$$3CaMg(CO_3)_2 + H_2O + 4SiO_2 \rightarrow MgSi_4O_{10}(OH)_2 + 3CO_2\uparrow + 3CaCO_3\downarrow \quad (1)$$

As the experimental water temperature increases, the intensity of the diffraction peak for the 5-phase product at 2θ=17.82° gradually decreases, initially starting from an intensity higher than that of the $Mg(OH)_2$ diffraction peak at 2θ=18.62°, until it falls below the intensity of the $Mg(OH)_2$ peak and eventually disappears. Similarly, the intensity of the $MgCO_3$ diffraction peak at 2θ=32.71° also gradually decreases. Notably, at 5 °C, the intensity of the $MgCO_3$

diffraction peak exceeds that of the $Mg(OH)_2$ peak at 2θ=32.71°. However, as the temperature rises, the MgCO3 peak intensity gradually diminishes to a level below that of $Mg(OH)_2$. Interestingly, at 30 °C, there is an increase in the intensity of the $MgCO_3$ diffraction peak, which coincides with a change in the strength of the sample. As the temperature continues to elevate, the number of phases present in the sample, particularly $Mg(OH)_2$ and $MgCO_3$, gradually decreases, with $Mg(OH)_2$ emerging as the dominant component. Consequently, this transformation leads to a decrease in the strength of the sample.

4.6 SEM analysis of YG-MOS foam concrete under different water temperatures

The scanning electron microscopy results of YG-MOS foamed concrete are shown in Fig. 8. The water temperatures corresponding to Figs. 8(a), 8(b), 8(c), and 8(d) are 5 °C, 35 °C, 50 °C, and 60 °C, respectively. When the water temperature is 5 °C, as shown in Fig. 8 (a), the overall structure of the sample is primarily composed of needle-like 5-phase crystals and flake-like $Mg(OH)_2$. The needle-like crystals are shorter, cross-distributed, and disordered. A minimal quantity of flake-like $Mg(OH)_2$ combines with the needle-like 5-phase crystals and fills the gaps between them, which is the main contributor to the strength of the structure. However, the structure appears loose, leading to a low strength of the sample.

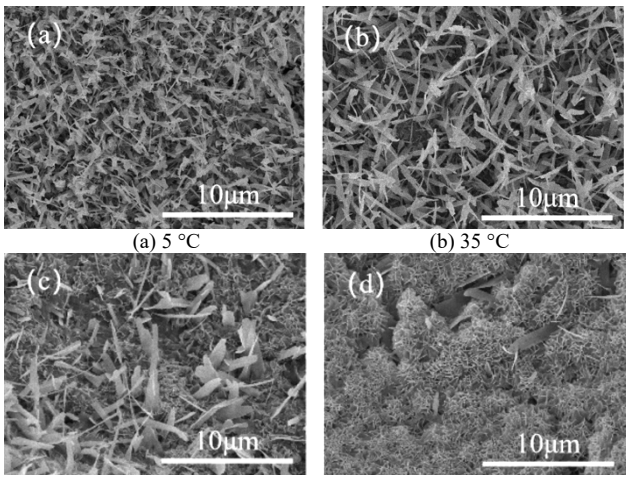

(a) 5 °C (b) 35 °C

(c) 50 °C (d) 60 °C

Fig. 8. SEM images of YG-MOS foam concrete at different water temperatures

When the water temperature is increased to 35 °C, as shown in Fig. 8(b), the needle-like 5-phase crystals combine with the flake-like $Mg(OH)_2$, resulting in increased crystal length and a cross-arranged structure. This leads to a denser overall structure and an increase in the strength of the sample. At 50 °C, as depicted in Fig. 8(c), the structure is predominantly composed of flake-like, petal-like, and cluster-like $Mg(OH)_2$, with very few 5-phase crystals present. Petal-like $Mg(OH)_2$ forms the main material and lies flat on the surface. Cluster-like $Mg(OH)_2$ is distributed within the petal-like $Mg(OH)_2$, and a minimal quantity of flake-like $Mg(OH)_2$ is dispersed between the petal-like structures. The arrangement is not tightly packed, with minimal crossover between the different forms of $Mg(OH)_2$. This results in a relatively loose overall structure. The structural strength is primarily provided by flake-like and petal-like $Mg(OH)_2$, contributing to a lower overall strength of the sample.

Finally, when the water temperature reaches 60 °C, as seen in Fig. 8(d), many cluster-like and petal-like $Mg(OH)_2$ structures are cross-arranged, with a minimal quantity of flake-like $Mg(OH)_2$ present within the cluster-like structures. The needle-like 5-phase crystal is not observable in the image. The structural strength is primarily provided by cluster-like and petal-like $Mg(OH)_2$, and the presence of gaps between $Mg(OH)_2$ further reduces the structural strength.

5. Conclusions

To promote the concept of green environmental protection and address the issues of land occupation and environmental pollution caused by the inadequate disposal of YG, an experimental study was conducted on the performance of YG-MOS foamed concrete at various water temperatures. The compressive strength, thermal conductivity, porosity, pore size, and microscopic mechanisms were analyzed. The main conclusions are obtained as follows:

(1) The influence of water temperature on the compressive strength of YG-MOS foamed concrete varies across different curing periods. Initially, over the first 24 h and up to 3 d, the change in strength is not pronounced. However, after 7 d of curing, the compressive strength of the samples initially increases but then decreases with increasing water temperature. Specifically, at 28 d of curing, the strength at 35 °C is 29% higher than that of samples cured at 5 °C. Above 35 °C, the compressive strength tends to decrease with further increases in temperature. Notably, at temperatures exceeding 45 °C, the compressive strength falls below that achieved at the initial experimental water temperature of 5 °C.

(2) The thermal conductivity of the samples initially increases and then decreases. At 35 °C, the maximum thermal conductivity is 0.2216 W/mK. If better thermal insulation performance is required, the water temperature can be reduced to achieve it. As the water temperature increases, both the average and standard deviation of the pore diameter of the samples initially decrease but then increase. At 35 °C, both reach their minimum values, with a mean pore size of 1.84 mm. At this point, the pore size distribution of the samples is the most uniform, resulting in favorable physical properties.

(3) As the water temperature increases, the dry density and porosity of the samples exhibit opposing trends. Initially, the porosity decreases and then increases with increasing water temperature. At 35 °C, the porosity reaches its minimum value of 61.72%. Conversely, the dry density first increases and then decreases with increasing water temperature. Specifically, at 35 °C, the dry density of the samples is 501.6 kg/m³, meeting the A05 dry density grade standards. These observations suggest that controlling the water temperature to approximately 35 °C can optimize the porosity and dry density of the samples.

(4) As the experimental water temperature increases, the XRD diffraction peak of the 5-phase product gradually weakens, while the peak of $Mg(OH)_2$ increases in intensity. The increase in experimental water temperature affects the crystal structure of the cementitious material. The structure of the samples gradually changes from a 5-phase structure to a magnesium hydroxide-dominated structure, which reduces the strength of the samples. When the temperature is between 5 °C and 35 °C, with increasing water temperature, the number and length of needle-like 5-phase structures in the samples increase. The $Mg(OH)_2$ and 5-phase structures combine to form a denser framework, leading to an increase

in compressive strength. As the experimental water temperature increases further, between 35 °C and 60 °C, the content of 5-phase structures in the samples gradually decreases, while the content of flake, cluster, and petal-shaped $Mg(OH)_2$ increases significantly.

This research demonstrates that a change in water temperature has a significant effect on the performance of YG-MOS foamed concrete. An appropriate water temperature can significantly enhance the behavior of YG-MOS foamed concrete. The incorporation of YG into MOS foamed concrete provides a novel approach for the treatment of YG as an industrial solid waste, which is conducive to promoting the concept of green environmental protection. Further studies are needed to investigate the influence of different YG contents and types of modifiers on YG-MOS foamed concrete. The next steps involve two main aspects: investigating the impact of varying YG contents on YG-MOS foamed concrete and examining the effects of different modifiers on the performance of YG-MOS foamed concrete.

Acknowledgments

This work was financially supported by the National Scholarship Fund of China [2023]-21, Key Project of Natural Science Foundation of Henan Province, China (232300421134), First-Class Discipline Implementation of Safety Science and Engineering (AQ20230103), and the Zhongyuan Science and Technology Innovation Leading Talent Program (244200510005), China.

References

[1] X. M. Guan, Z. H. Zhang, H. F. Di, and S. H. Liu, "Effect of type II anhydrite prepared by different methods of titanium gypsum on the properties of sulphoaluminate cement," *J. Henan Polytech. Univ. (Nat. Sci. Ed.)*, vol. 43, no. 02, pp. 194-200, Sep. 2023. doi:10.16186/j.cnki.1673-9787.2023020070.

[2] Z. Wang, G. Chen, L. Li, L. J. Wang, and J. Ma, "Background and prospect of technical standard for comprehensive utilization of titanium gypsum," *China Coat*, vol. 38, no. 11, pp. 1-7, Nov. 2023. doi:10.13531/j.cnki.china.coatings.2023.11.001.

[3] X. J. Pan and J. Li, "The characteristics and application of foamed concrete and its future development trend," *Concrete Cement Products*, no. 06, pp. 98-102, Jun. 2020. doi:10.19761/j.1000-4637.2020.06.098.05.

[4] J. Gong, Q. Q. Liu, S. R. Wang, Z. X. Wang, and C. L. Li, "Mechanical properties and microscopic mechanism of paper mill sludge-magnesium oxychloride cement composites," *Dyna*, vol. 98, no. 1, pp. 57-63, Jan. 2023. doi:10.6036/10714.

[5] S. R. Wang, J. L. Wei, X. Y. Wang, and J. Wang, "Experimental study on influence of ultra-fine cement content on mechanical properties of modified sludge", *J. Eng. Scie. Technol. Re.*, vol.14, no. 2, pp. 44-53, Apr. 2021. doi:10.25103/jestr.142.06.

[6] J. M. Dassekpo, C. Zhang, J. Bai, D. Y. Liu, Y. R. Li, Z. J. Dong, and F. Xing, "Alkali-activation of calcined granitic waste: Reaction mechanisms and environmental implication for waste minimization," *Constr. Build. Mater.*, vol. 327, Apr. 2022, Art. no. 126976. doi:10.1016/j.conbuildmat.2022.126976.

[7] S. R. Wang, Z. X. Wang, J. Gong, and Q. Q. Liu, "Damage mode and energy consumption characteristics of paper sludge doped magnesium chloride cement composites," *Sustainability*, vol. 15, no. 17, Aug. 2023, Art. no. 13051. doi:10.3390/su151713051.

[8] J. R. Ju, Y. L. Feng, H. R. Li, and C. L. Xu, "Resource utilization of strongly acidic wastewater and red gypsum by a harmless self-treatment process," *Process Saf. Environ.*, vol. 172, pp. 594-603, Apr. 2023. doi:10.1016/j.psep.2023.02.067.

[9] N. M. Marian, M. Perotti, C. Indelicato, C. Magrini, G. Giorgetti, G. Capitani, and C. Viti, "From high-volume industrial waste to new ceramic material: The case of red gypsum muds in the TiO_2 industry," *Ceram. Int.*, vol. 49, no. 10, pp. 15034-15043, May 2023. doi:10.1016/j.ceramint.2023.01.086.

[10] E. Namsone, G. Sahmenko, and A. Korjakins, "Properties of magnesium oxychloride and magnesium oxysulphate cement composites," *Key Eng. Mater.*, vol. 903, pp. 208-213, Nov. 2021. doi:10.4028/www.scientific.net/KEM.903.208.

[11] J. Zapata-Carbonell, C. Bégeot, N. Carry, F. Choulet, P. Delhautal, F. Gillet, O. Girardclos, A. Mouly, and M. Chalot, "Spontaneous ecological recovery of vegetation in a red gypsum landfill: Betula pendula dominates after 10 years of inactivity," *Ecol. Eng.*, vol. 132, pp. 31-40, Jul. 2019. doi:10.1016/j.ecoleng.2019.03.013.

[12] N. A. Rosli, H. A. Aziz, M. R. Selamat, L. L. P. Lim, and M. H. Zawawi, "Effect of compaction on physical properties of a sewage sludge and red gypsum mixture as intermediate landfill cover," *Constr. Build. Mater.*, vol. 289, Jun. 2021, Art. no. 123153. doi:10.1016/j.conbuildmat.2021.123153.

[13] K. Sotiriadis, P. I. Kiyko, T. N. Chernykh, and M. V. Kriushin, "Self-cleaning ability of gypsum-cement-pozzolan binders based on thermally processed red gypsum waste of titanium oxide manufacture," *J. Build. Eng.*, vol. 87, Jun. 2024, Art. no. 109009. doi:10.1016/j.jobe.2024.109009.

[14] S. R. Wang, L. R. Zhao, J. Gong, M. Lutynski, Y. Wang, and C. L. Li, "Experimental research on mechanical properties of magnesium oxychloride-based titanium gypsum concrete," *Dyna*, vol. 99, no. 2, pp. 215-220, Mar. 2024. doi:10.6036/11171.

[15] K. Gu, B. Chen, H. F. Yu, N. Zhang, W. L. Bi, and Y. Guan, "Characterization of magnesium-calcium oxysulfate cement prepared by replacing MgSO4 in magnesium oxysulfate cement with untreated desulfurization gypsum," *Cement Concrete Comp.*, vol. 121, Aug. 2021, Art. no. 104091. doi:10.1016/j.cemconcomp.2021.104091.

[16] M. X. Li, K. Gu, and B. Chen, "Effects of flue gas desulfurization gypsum incorporation and curing temperatures on magnesium oxysulfate cement," *Constr. Build. Mater.*, vol. 349, Sep. 2022. Art. no. 128718. doi:10.1016/j.conbuildmat.2022.128718.

[17] K. Y. Fang, C. Y. Wu, and H. D. Chen, "The Influences and Effect Mechanism of Low Temperature Curing on the Performances of Basic Magnesium Sulfate Cement," *J. Adv. Concr. Technol.*, vol. 21, no. 12, pp. 995-1007, Dec. 2023. doi:10.3151/jact.21.995.

[18] L. F. Rodríguez-Alfaro, L. M. Torres-Martínez, M. Z. Treviño-Garza, J. M. Vázquez-Guillén, C. Rodríguez-Padilla, and E. Luévano-Hipólito, "Exploring the self-cleaning and antimicrobial efficiency of the magnesium oxychloride cement composites," *Ceram. Int.*, vol. 49, no. 13, pp. 21370-21383, Jul. 2023. doi:10.1016/j.ceramint.2023.03.266

[19] A. K. Dionisio, and C. M. Gomes, "Behaviour of autoclaved magnesium oxysulfate cement pastes," *J. Build. Eng.*, vol. 76, Oct. 2023, Art. no. 107263. doi:10.1016/j.jobe.2023.107263.

[20] W. Y. Li, J. B. Zhou, Z. Y. Zhang, and X. X. Zhu, "Study on preparation and properties of red mud magnesium oxysulfate cement foamed concrete," *Bull. Environ. Contam. Toxicol.*, vol. 109, no. 1, pp. 130-134, Jul. 2022. doi:10.1007/s00128-022-03521-7.

[21] J. W. Jiang, X. Zhang, Q. L. Liu, C. B. Lei, J. G. Ren, "Effect of rice straw on properties of magnesium oxysulfate foam lightweight thermal insulation material," *Concrete and Cement Products*, no .03, pp. 91-95, Mar. 2023. doi:10.19761/j.1000-4637.2022.03.091.05.

[22] J. Gong, Q. Q. Liu, S. R. Wang, Z. X. Wang, and C. L. Li, "Effects of modifiers on magnesium oxychloride cement doped with paper mill sludge," *Dyna*, vol. 98, no. 5, pp. 492-497. Sept. 2023. doi:10.6036/10968.